
Manganese Carboxylate Clusters as Single-Molecule Magnets (Molecular Nanomagnets)

George Christou

Department of Chemistry, University of Florida
Gainesville, FL 32611-7200, USA

christou@chem.ufl.edu

Advantages of SMMs over Classical Nanoscale Magnetic Particles

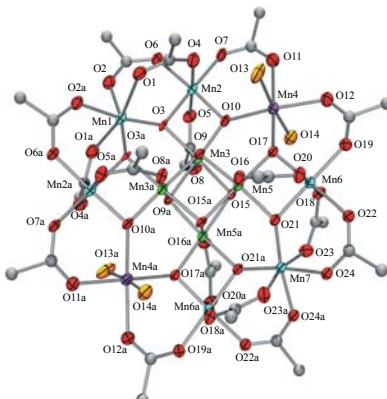
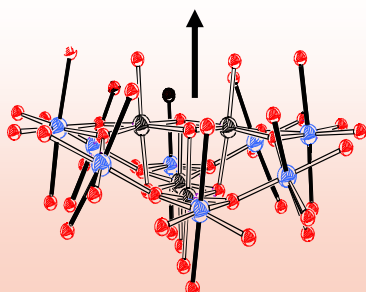
- ❑ A collection of truly monodisperse particles of nanoscale dimensions
- ❑ Crystalline, containing highly ordered assemblies of SMMs
- ❑ A single, well-defined ground state spin, S
- ❑ A true quantum spin system
- ❑ Synthesis by room temperature, solution methods
- ❑ Enveloped in protective shell of organic groups
- ❑ True solubility (rather than colloidal suspension) in organic liquids
- ❑ Easy chemical modification of organic shell

Requirements for Single-Molecule Magnets:

1. Large spin ground state (S)
2. Large and negative magnetic anisotropy (negative zero-field splitting parameter, D)

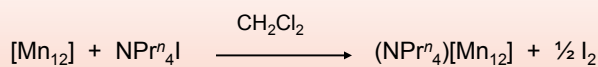
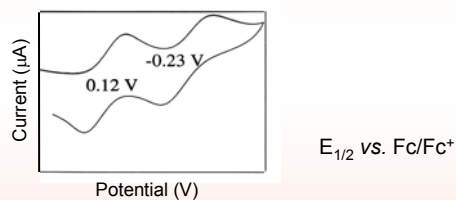
$[\text{Mn}_{12}\text{O}_{12}(\text{O}_2\text{CR})_{16}(\text{H}_2\text{O})_4]$ complexes:

- S = 10
- D = -0.40 to -0.50 cm⁻¹ = 58 to 72 K
- Magnet below 3K
- R group easily varied at will



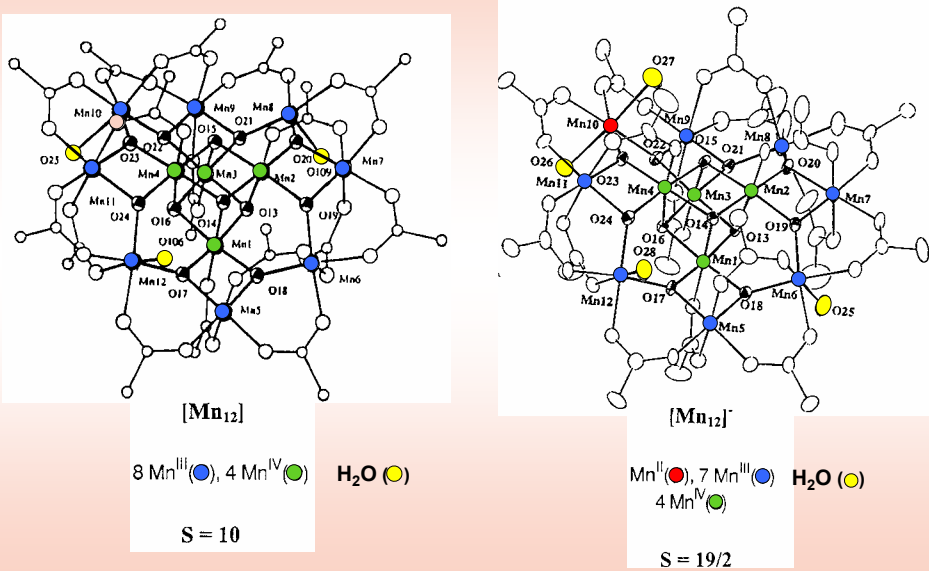
One-electron Reduction of Mn_{12} Complexes

- Mn_{12} complexes reduced with one electron have been previously prepared and studied, e.g. $(\text{PPh}_4)[\text{Mn}_{12}\text{O}_{12}(\text{O}_2\text{CEt})_{16}(\text{H}_2\text{O})_4]$
- $[\text{Mn}_{12}]^-$ have S = 19/2 ground states; a few have S = 21/2
- Electrochemistry studies: CV of $[\text{Mn}_{12}\text{O}_{12}(\text{O}_2\text{CPh})_{16}(\text{H}_2\text{O})_4]$



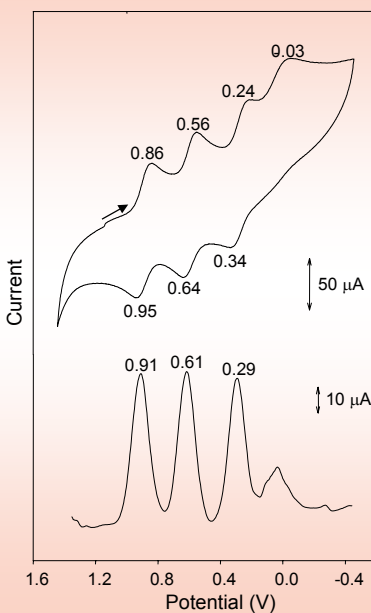
Eppley *et al.* JACS, 1995

Crystal Structures of Mn_{12} and $[\text{Mn}_{12}]^-$



Eppley et al. JACS, 1995

CV and DPV Data for $[\text{Mn}_{12}\text{O}_{12}(\text{O}_2\text{CCHCl}_2)_{16}(\text{H}_2\text{O})_4]$

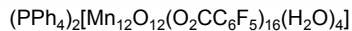
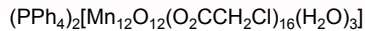
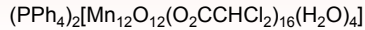
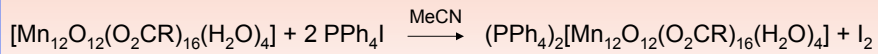


Electrochemical data for
 $[\text{Mn}_{12}\text{O}_{12}(\text{O}_2\text{CR})_{16}(\text{H}_2\text{O})_4]$

R	E_1 (V) ^a	E_2 (V) ^b
CHCl_2 (5)	0.91	0.61
$\text{C}_6\text{H}_3(\text{NO}_2)_2\text{-2,4}$ (7)	0.74	0.45
C_6F_5 (8)	0.64	0.46
CH_2Cl (6)	0.60	0.30

In MeCN. E_i (V) are DPV peaks. ^aFirst reduction.
^bSecond reduction. Referenced vs. Fc/Fc^+

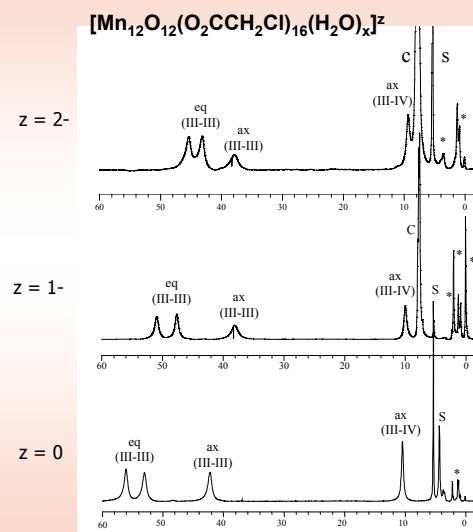
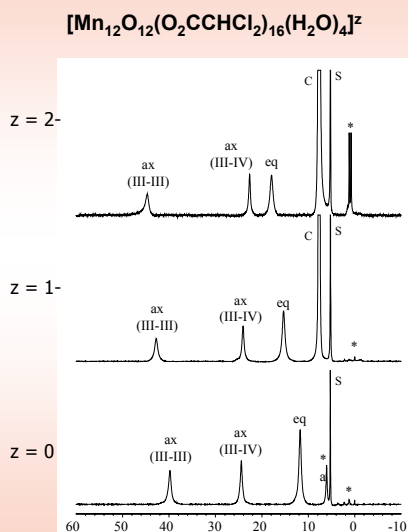
Two-electron Reduction of Mn_{12} Complexes to $[\text{Mn}_{12}]^{2-}$



Characterization:

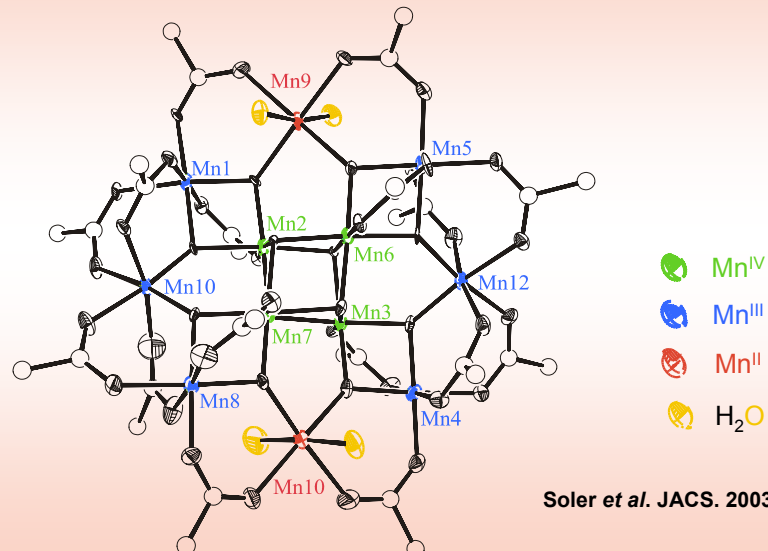
- IR, ^1H NMR and ^{19}F NMR spectra
- Electrochemical studies : Cyclic Voltammogram (CV)
Differential Pulse Voltammogram (DPV)
- Elemental analyses
- Crystal structures
- Magnetism studies

^1H NMR Spectra of $[\text{Mn}_{12}]^{2-}$ in CD_3CN Solution



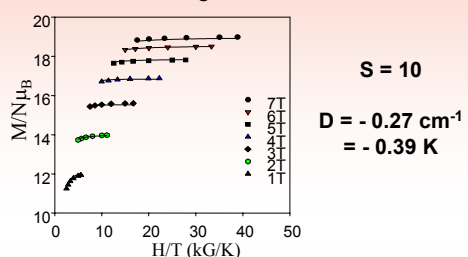
Effective solution symmetry D_{2d}

$(\text{PPh}_4)_2[\text{Mn}_{12}\text{O}_{12}(\text{O}_2\text{CCHCl}_2)_{16}(\text{H}_2\text{O})_4] \cdot 4\text{CH}_2\text{Cl}_2 \cdot \text{H}_2\text{O}$ (10)

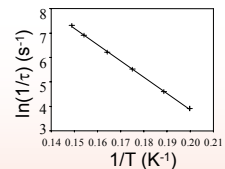
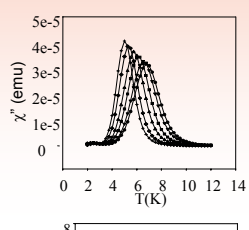


Magnetic Properties of $[\text{Mn}_{12}]^{2-}$

DC Reduced Magnetization



AC Susceptibility



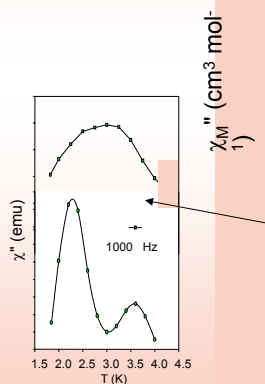
$$\ln\left(\frac{1}{\tau}\right) = \ln\left(\frac{1}{\tau_0}\right) + \frac{-U_{\text{eff}}}{k} \frac{1}{T}$$

Arrhenius plot $\rightarrow U_{\text{eff}}$

	$[\text{Mn}_{12}]$	$[\text{Mn}_{12}]^{1-}$	$[\text{Mn}_{12}]^{2-}$
\mathbf{S}	10	19/2	10
\mathbf{D} (K)	-0.65	-0.49	-0.39
\mathbf{U}_{eff} (K)	66	57	32

Out-of-Phase AC Susceptibility for Mn_{12} , $[\text{Mn}_{12}]^-$ and $[\text{Mn}_{12}]^{2-}$

- for dried solids



Mn_{12}

χ_M'' peak at 6 - 8 K

$[\text{Mn}_{12}]^-$

χ_M'' peak at 4 - 6 K

$[\text{Mn}_{12}]^{2-}$

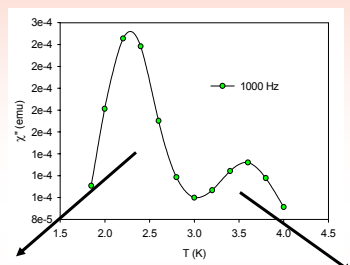
χ_M'' peak at 2 - 4 K

Out-of-phase AC Magnetic Susceptibility for $(\text{PPh}_4)_2[\text{Mn}_{12}\text{O}_{12}(\text{O}_2\text{CCHCl}_2)_{16}(\text{H}_2\text{O})_4]$



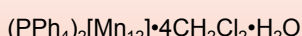
Peak at 2.4 K

Arrhenius $\rightarrow U_{\text{eff}} = 18.5 \text{ K}$

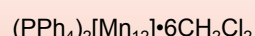


Peak at 3.6 K

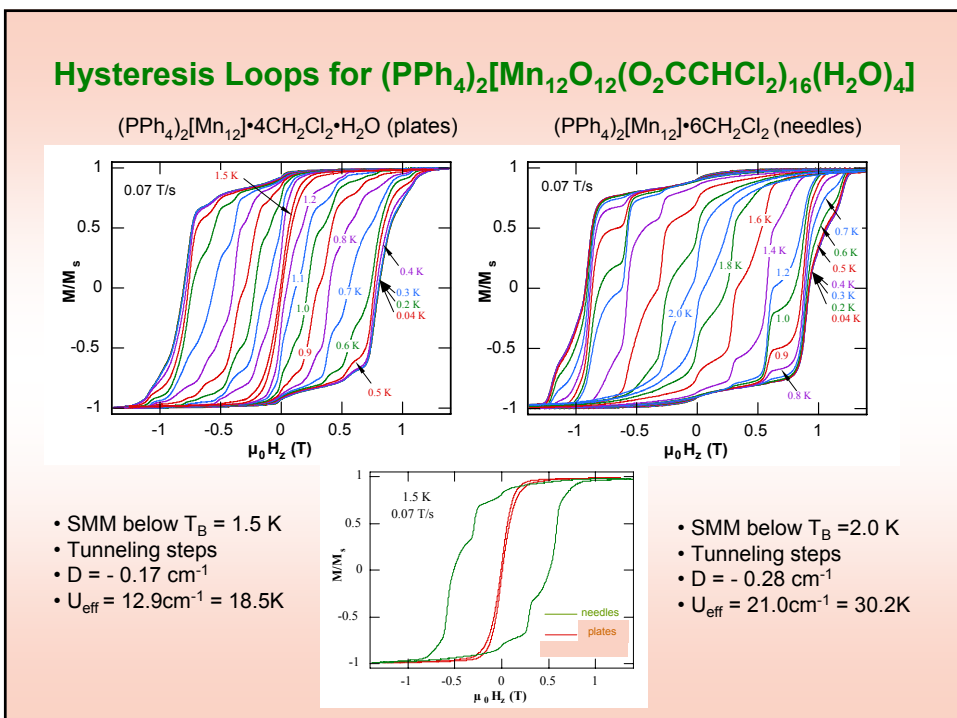
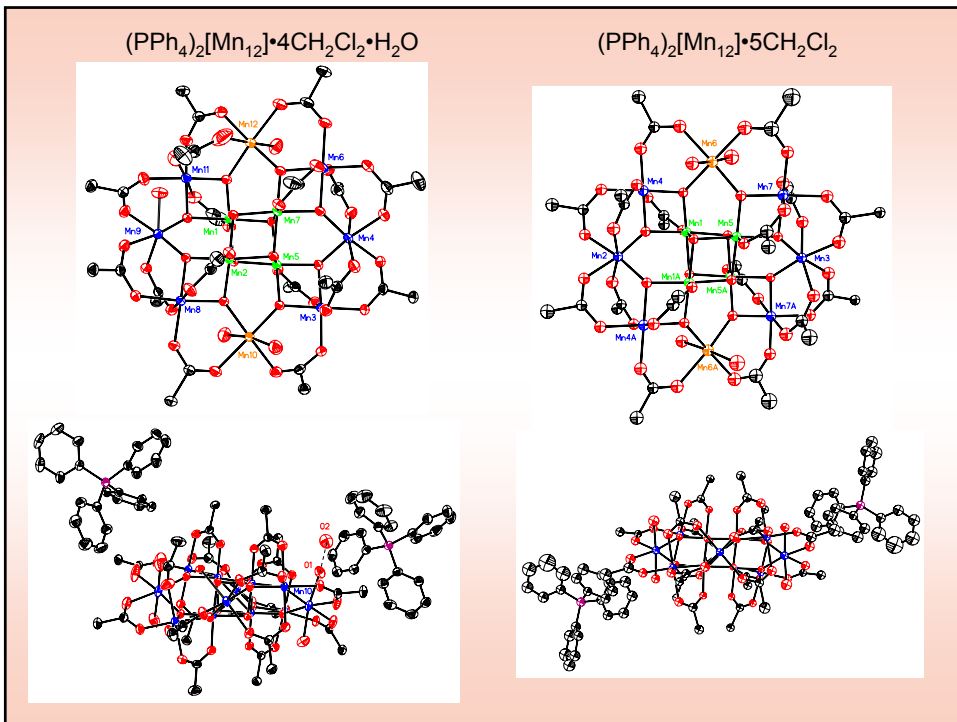
Arrhenius $\rightarrow U_{\text{eff}} = 30.2 \text{ K}$



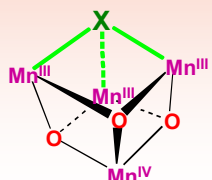
triclinic $P\bar{1}$
 $V = 6969.79 \text{ \AA}^3$



Monoclinic $P2_1/c$
 $V = 7468.51 \text{ \AA}^3$

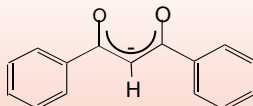


Mn_4 SMMs with $S = 9/2$



- $3\text{Mn}^{\text{III}}, \text{Mn}^{\text{IV}}$
- C_{3v} virtual core symmetry
- Mn^{3+} Jahn-Teller axial elongations
- Core ligands (X): Cl^- , Br^- , F^-
 NO_3^- , N_3^- , NCO^-
 OH^- , MeO^- , Me_3SiO^-

- Peripheral ligands: (i) carboxylate ligands: O_2CMe , O_2CEt

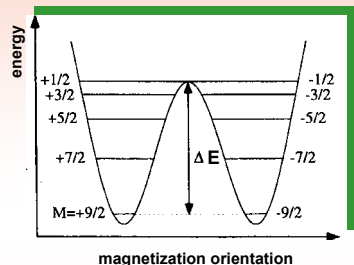


- (ii) Cl^- , py, HIm, dbm $^-$, Me_2dbm^- , Et_2dbm^-

Properties of Mn_4 SMMs with $S = 9/2$

SMMs: Single-Molecule Magnets

- A significant S value. $S = 9/2$
- Easy axis (Ising) type anisotropy
 $D = -0.65$ to -0.75 K
- $\Delta E = (S^2 - 1/4)|D| = 20$ D

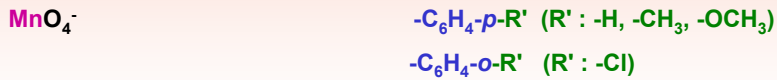


Advantages

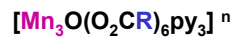
- Variation in core X group, with constant ligand groups
- Variation in ligand R groups, for a given $\text{Mn}_4\text{O}_3\text{X}$ core.
- Soluble in organic solvents.
- Sub-nanoscale dimensions (core volume $\sim 0.01 \text{ nm}^3$).

Synthesis Routes to Mn₄ Complexes

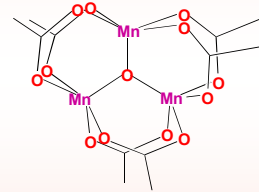
Mononuclear compounds:



Trinuclear compounds:



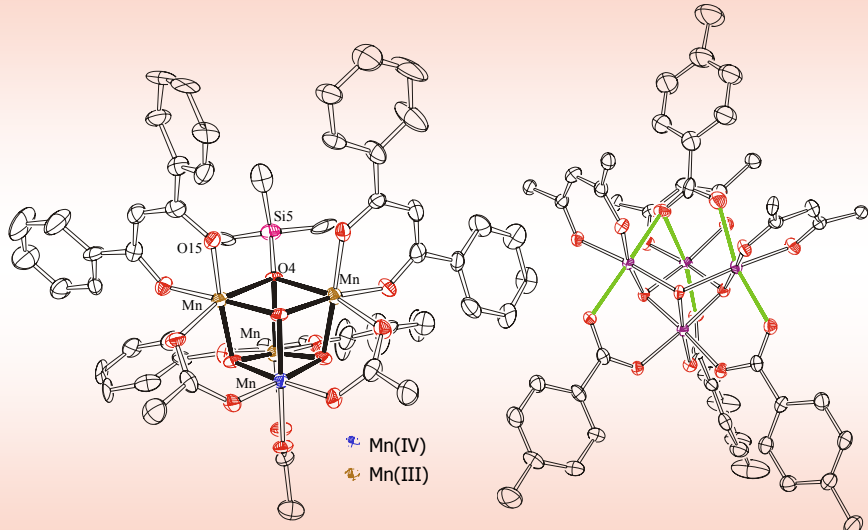
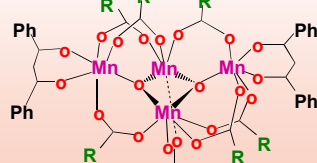
where n = 0, +1



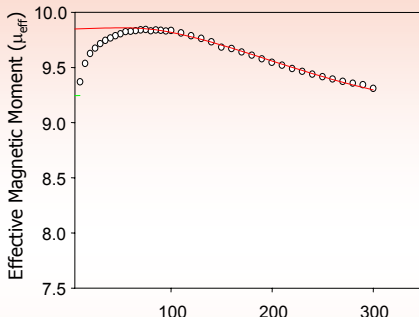
Tetranuclear compounds:



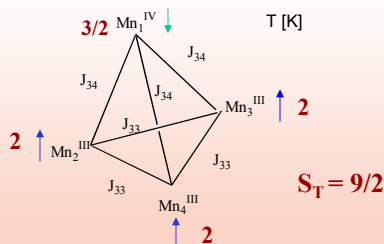
where n = 0, -1



Exchange Parameters in Mn_4 SMMs



X	OSiMe₃
J_{34} (cm ⁻¹)	-34.35
J_{33} (cm ⁻¹)	+13.41
<i>g</i>	1.97
<i>S</i>	9/2
1 st ex. st	264 cm ⁻¹



$$H = -2J_{33}(\hat{S}_2\hat{S}_3 + \hat{S}_2\hat{S}_4 + \hat{S}_3\hat{S}_4) - 2J_{34}(\hat{S}_1\hat{S}_2 + \hat{S}_1\hat{S}_3 + \hat{S}_1\hat{S}_4)$$

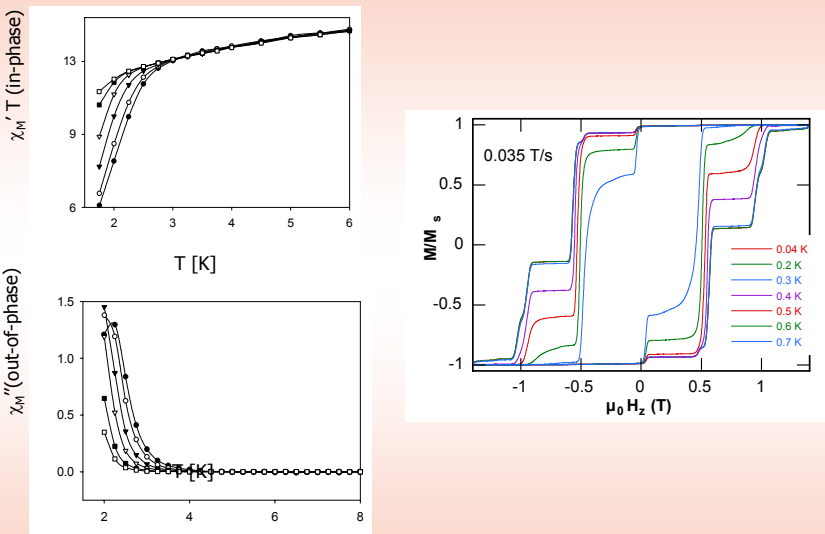
$$S_T = 9/2$$

Properties of $[\text{Mn}_4\text{O}_3\text{X}(\text{O}_2\text{CR})_3(\text{dbm})_3]$ Complexes

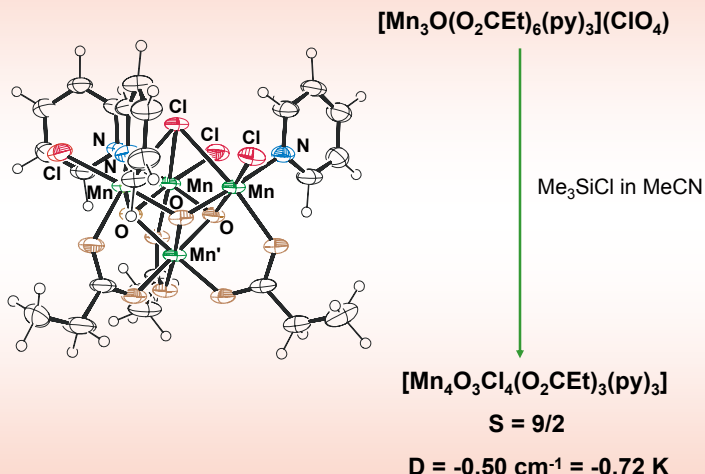
--from magnetization vs H and T fits

X	Cl	Br	MeCO₂	PhCO₂
J_{34} (cm ⁻¹)	-28.4	-30.1	-33.9	-28.5
J_{33} (cm ⁻¹)	+8.3	+7.4	+5.4	+2.8
J_{33} (cm ⁻¹)	-	-	-	+2.1
Ground State	9/2	9/2	9/2	9/2
D, cm⁻¹ (K)	-0.53(-0.76)	-0.50(-0.72)	-0.47(-0.68)	-0.58(-0.83)
1st Excited State	7/2	7/2	7/2	7/2
E(7/2), K	266	257	240	164

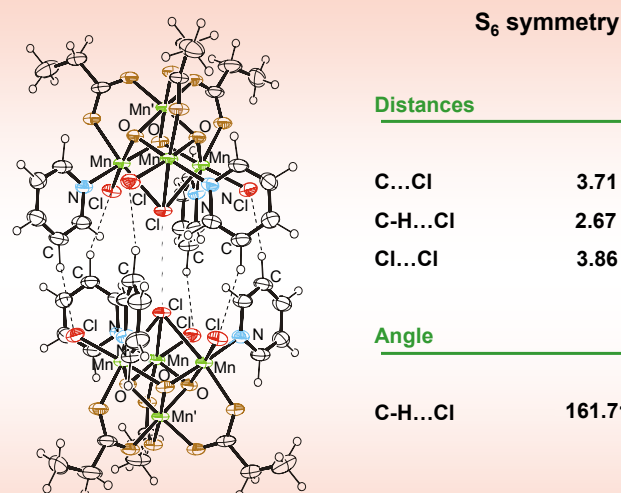
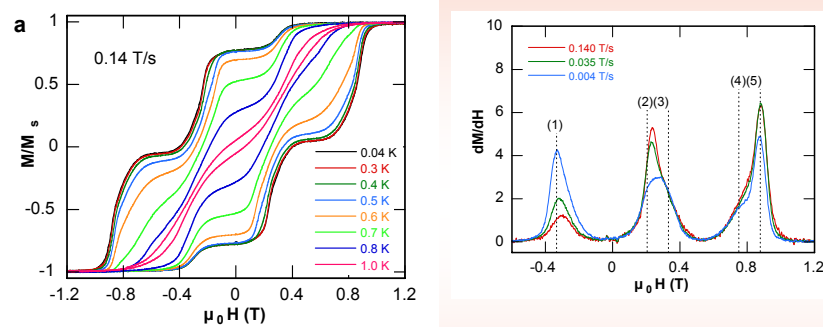
AC Magnetic Susceptibility & Hysteresis Loops for Mn₄Si (SB1)



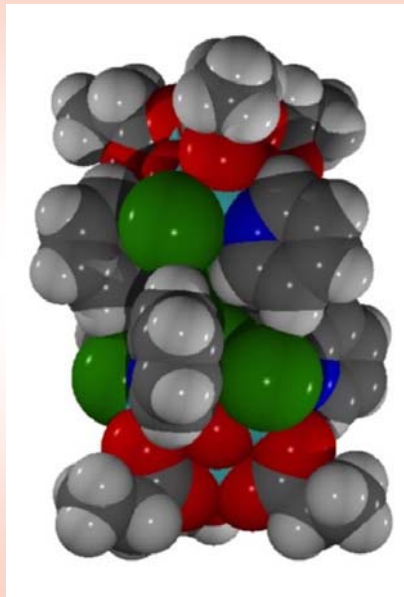
Mn₄ SMMs with $S = 9/2$ (NA3)



Hysteresis loops for $[\text{Mn}_4\text{O}_3\text{Cl}_4(\text{O}_2\text{CEt})_3(\text{py})_3]$



W. Wernsdorfer, N. Aliaga-Alcalde, D. N. Hendrickson, and G. Christou, *Nature*, **2002**, 406-409



$$H_i = D \hat{S}_{zi}^2 + H_i^{trans} + g \mu_B \mu_0 \hat{S}_{zi} H_z$$

$i = 1$ or 2

D = axial anisotropy constant,

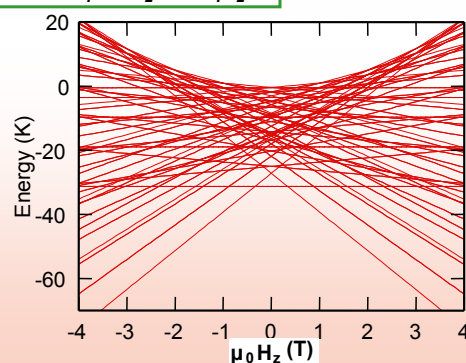
H_i^{trans} = small transverse anisotropy contains \hat{S}_{xi} and \hat{S}_{yi} spin operators.

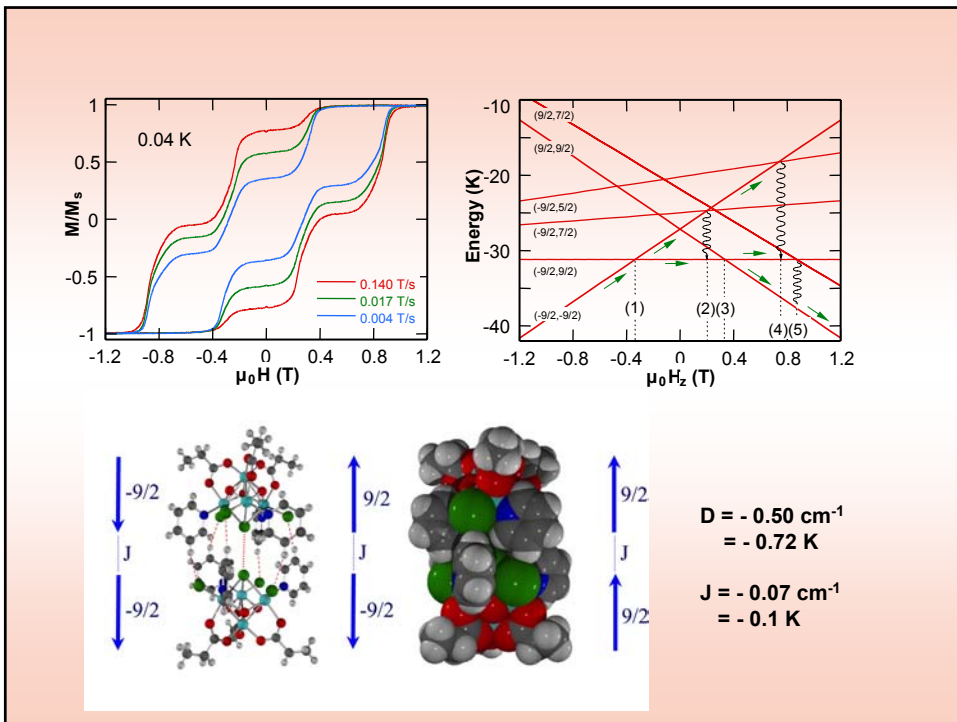
$g \mu_B \mu_0 \hat{S}_{zi} H_z$ = Zeeman energy associated with an applied field.

$$H = H_1 + H_2 + J \hat{S}_1 \hat{S}_2$$

$$\hat{S}_1 = \hat{S}_2 = \frac{9}{2}$$

$$(2S_1+1)(2S_2+1) = 100$$

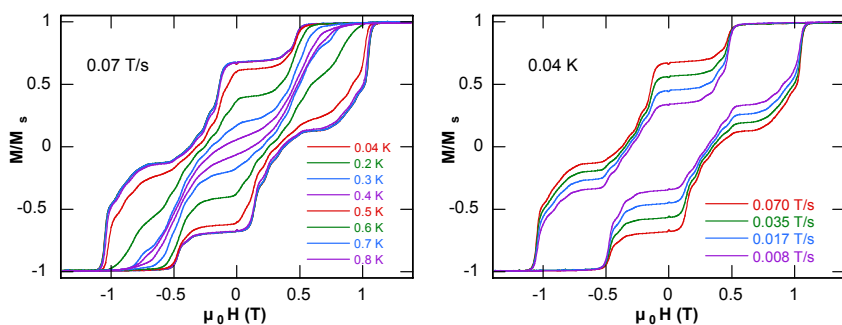




$[\text{Mn}_4\text{O}_3\text{Cl}_4(\text{O}_2\text{CR})_3(\text{NC}_5\text{H}_4-\text{p-R'})_3]$ $S = 9/2$					
	$\text{R} = \text{Me}$ $\text{R}' = \text{H}$	$\text{R} = \text{Et}$ $\text{R}' = \text{H}$	$\text{R} = \text{Et}$ $\text{R}' = \text{H}$	$\text{R} = \text{Et}$ $\text{R}' = \text{D}$	$\text{R} = \text{Et}$ $\text{R}' = \text{t-butyl}$
Sp. Group	R3bar	R3bar	R3bar	R3bar	P2 ₁ /n
Temp(°C)	118	130	173	173	173
Cryst. Solvent	NA2 MeCN	NA3 MeCN	CH ₂ Cl ₂ / Et ₂ O Hexanes	NA3Deut MeCN	MeCN
(Å) Cl ⋯ Cl	3.739(13)	3.858(12)	3.712(10)	3.844(7)	3.884(9)
(Å) Cl ⋯ C	3.600	3.706	3.664	3.721	3.675 3.688 3.607
(°) C-H⋯Cl	158.15	158.00	151.94	157.36	163.32 160.03 157.72
(Å) Mn ^{III} ⋯Mn ^{III}	7.630	7.788	7.622	7.750	7.750

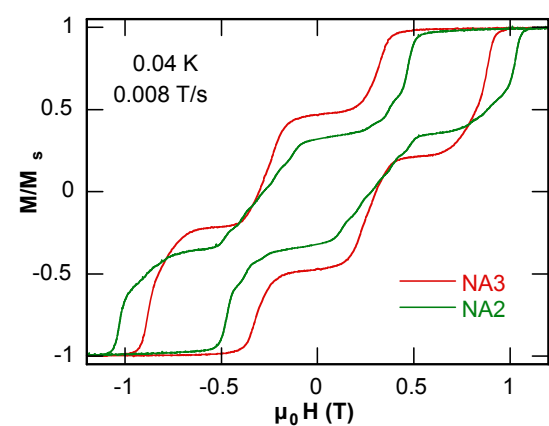
Hysteresis loops for $[\text{Mn}_4\text{O}_3\text{Cl}_4(\text{O}_2\text{CMe})_3(\text{py})_3]$

(NA2 or $[\text{Mn}_4\text{Ac}]_2$)



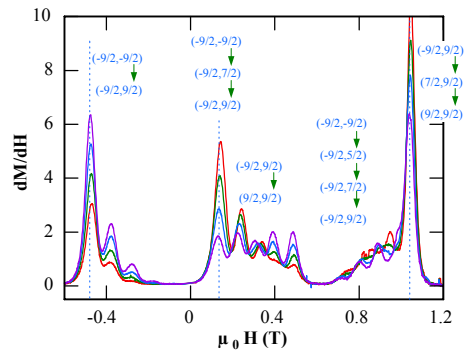
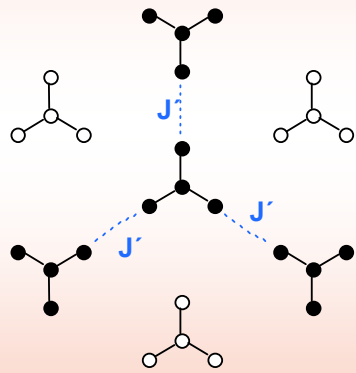
Comparison of $[\text{Mn}_4\text{Ac}]_2$ and $[\text{Mn}_4\text{Pr}]_2$

(NA2) (NA3)

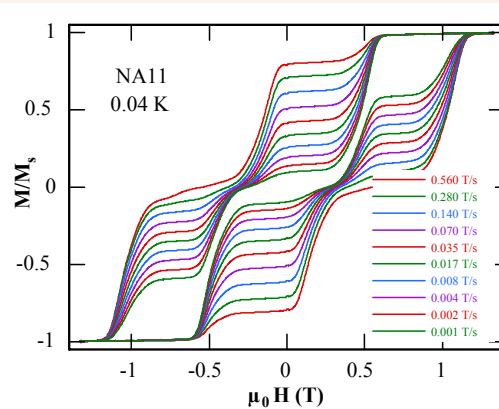


$J \approx 0.1 \text{ K}$ for $[\text{Mn}_4\text{Pr}]_2$ (NA3) and $J \approx 0.13 \text{ K}$ for $[\text{Mn}_4\text{Ac}]_2$ (NA2)

Fine structure evidence for inter-dimer exchange interactions

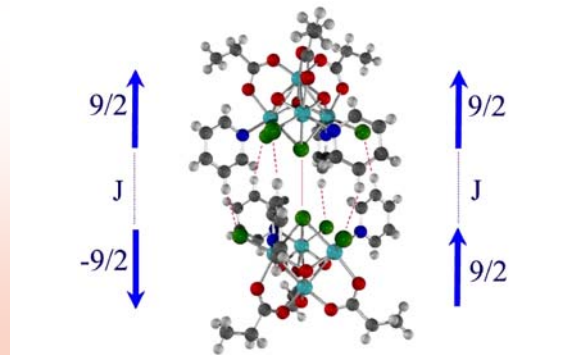


Hysteresis Loops for $\text{Mn}_4\text{O}_3\text{Cl}_4(\text{O}_2\text{CEt})_3(\text{py})_3$ [Mn₄Pr]₂ or NA11

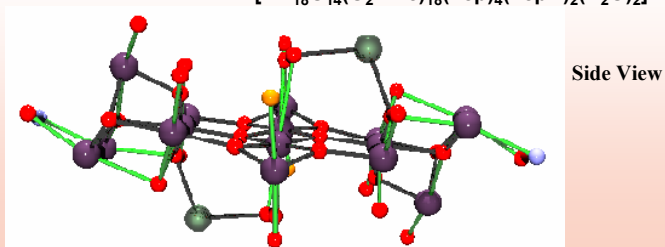
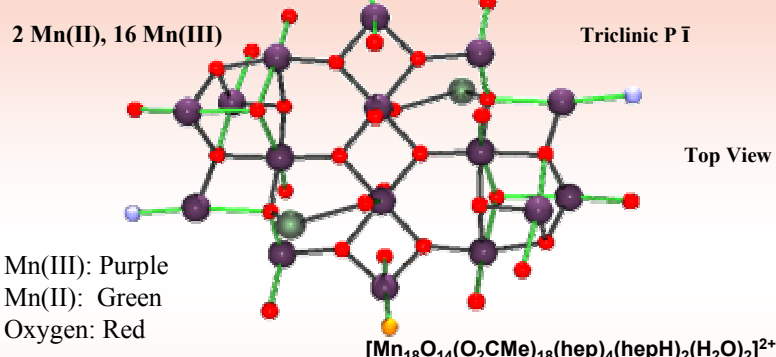


Advantages of Exchange-biased QTM

- tuning quantum properties (no QTM at zero field)
- coupled system with $S = 0$
- model system for magnetization tunnelling in mesoscopic antiferromagnets
- potential applications as a quantum bit
- establishes supramolecular chemistry can be used to modulate quantum physics of SMMs in a controlled way



A Mn_{18} Single-Molecule Magnet with $S = 13$



$[\text{Mn}_{18}\text{O}_{14}(\text{O}_2\text{CMe})_{18}(\text{hep})_4(\text{hepH})_2(\text{H}_2\text{O})_2]^{2+}$

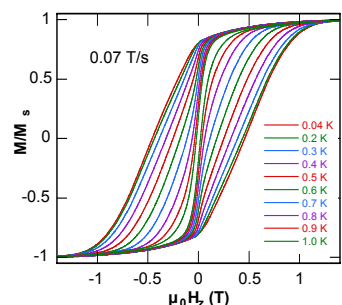
From M/μ_B vs H/T fits:

$$S = 13 \quad g = 1.86$$

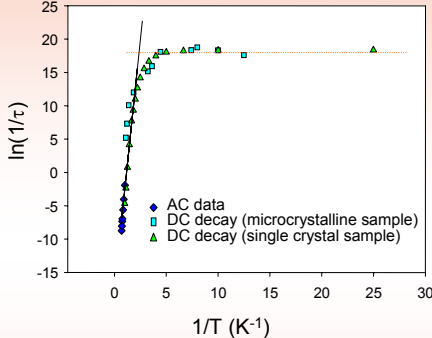
$$D = -0.13 \text{ cm}^{-1} = -0.19 \text{ K}$$

$$U = S^2 |D| = 32 \text{ K}$$

Hysteresis Loops at <1.0 K



Arrhenius Plot 0.04 – 2.0 K



Fit of the T-dependent data >0.2K

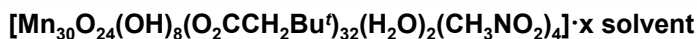
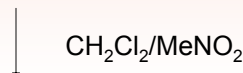
$$U_{\text{eff}} = 14.8 \text{ cm}^{-1} = 21.3 \text{ K}$$

Fit of the T-independent data <0.2K

$$\tau = 1.3 \times 10^{-8} \text{ s}^{-1} = \text{tunneling rate}$$

Largest cluster and largest S to show QTM

A Mn₃₀ SMM from a Mn₁₂ Precursor Complex



Characterization:

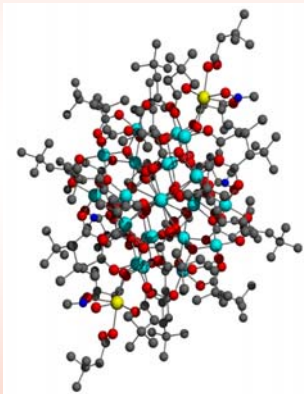
- IR
- Elemental analysis
- Crystal structures
- Magnetism studies

A Mn₃₀ Single-Molecule Magnet

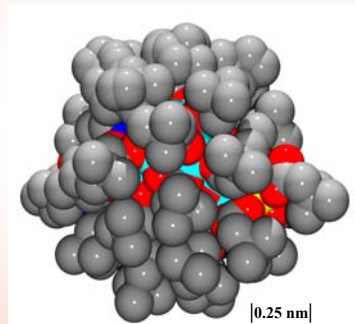


3Mn²⁺, 26 Mn³⁺, Mn⁴⁺

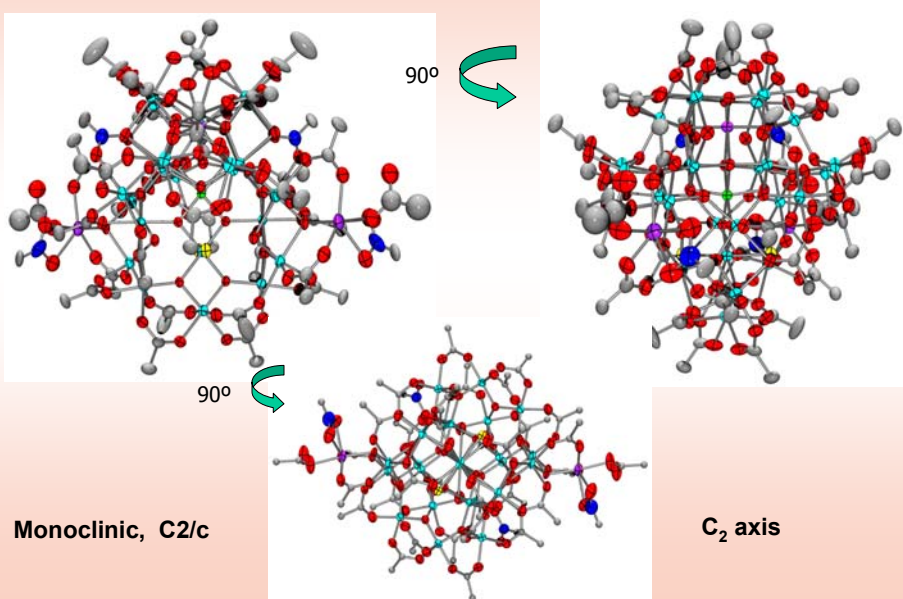
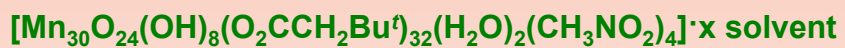
Monoclinic C2/c



Ball-and-stick View

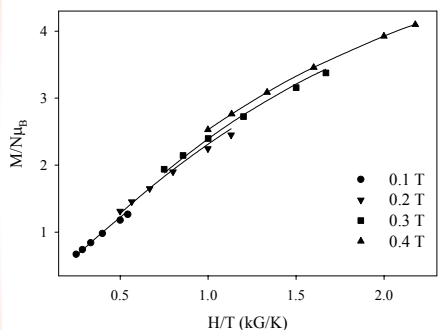


Space-filling View

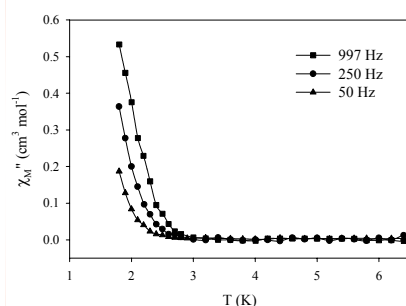


DC and AC Susceptibility Studies on Mn₃₀

DC Magnetization vs H and T



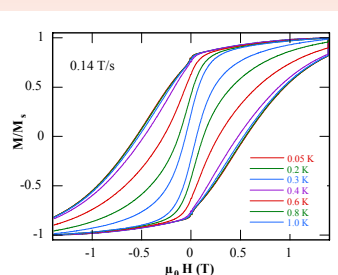
Out-of-phase AC susceptibility



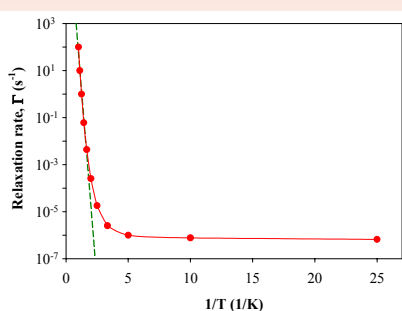
$S = 5$, $D = -0.51 \text{ cm}^{-1} = -0.73 \text{ K}$, and $g = 2$
 Calculated relaxation barrier (U) = $S^2 D = 13 \text{ cm}^{-1} = 18 \text{ K}$

Hysteresis Loops and DC Relaxation Data for Mn₃₀

Hysteresis Loops



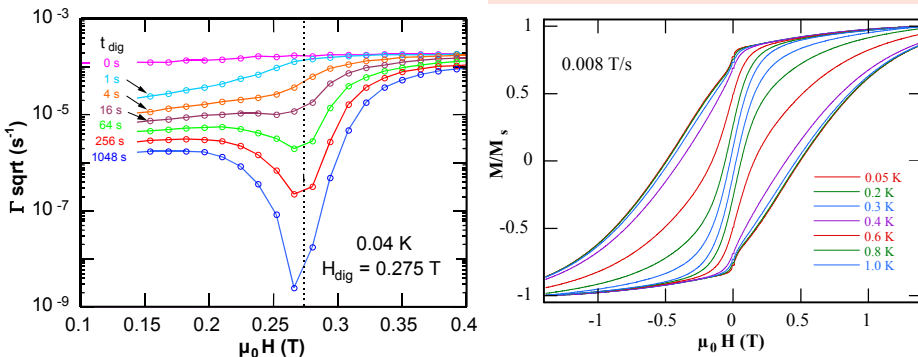
Arrhenius plot (from M vs t decay)



- Mn₃₀ is a SMM
- Blocking temperature (T_B) of $\sim 1.2 \text{ K}$
- Distribution of barriers (D values)
 (absence of well defined quantum steps)
- QTM step at zero field just visible

$U_{\text{eff}} = 15 \text{ K}$, thus $U_{\text{eff}} < U$ (18 K)
 below 0.2 K, relaxation rate is T
 independent \rightarrow tunneling

Quantum Hole-digging Method to detect QTM



- If QTM can occur in Mn_{30} , then that fraction and only that fraction of molecules that are in resonance at H_{dig} can tunnel
- the ‘hole’ in the plot reflects the distribution of spins still available for tunneling after t_{dig}

Summary

- $[\text{Mn}_{12}]^{2-}$ complexes with strongly electron-withdrawing substituents can be isolated. They have $S = 10$ and are SMMs like Mn_{12}^-
- Two crystal forms of the $[\text{Mn}_{12}]^{2-}$ complex with $\text{Cl}_2\text{CHCO}_2^-$ have significantly different magnetization relaxation barriers caused by different D values. SMM properties are very sensitive to the environment!
- Their hysteresis loops confirm the different relaxation barriers, and exhibit quantum tunneling of the magnetization (QTM)
- Mn_4 SMMs with $S = 9/2$ unequivocally establish that weak intermolecular exchange interactions have a significant influence on QTM, which suggests a means of fine-tuning QTM using this exchange-bias effect
- New $[\text{Mn}_{18}]^{2+}$ and Mn_{30} SMMs have been discovered with $S = 13$ and $S = 5$, respectively. $[\text{Mn}_{18}]^{2+}$ is the largest spin (S) cluster to show quantum tunneling of magnetization. Mn_{30} is the largest size cluster to show QTM